Neuron, Volume *107*

Supplemental Information

A Neural Network

for Wind-Guided Compass Navigation

Tatsuo S. Okubo, Paola Patella, Isabel D'Alessandro, and Rachel I. Wilson

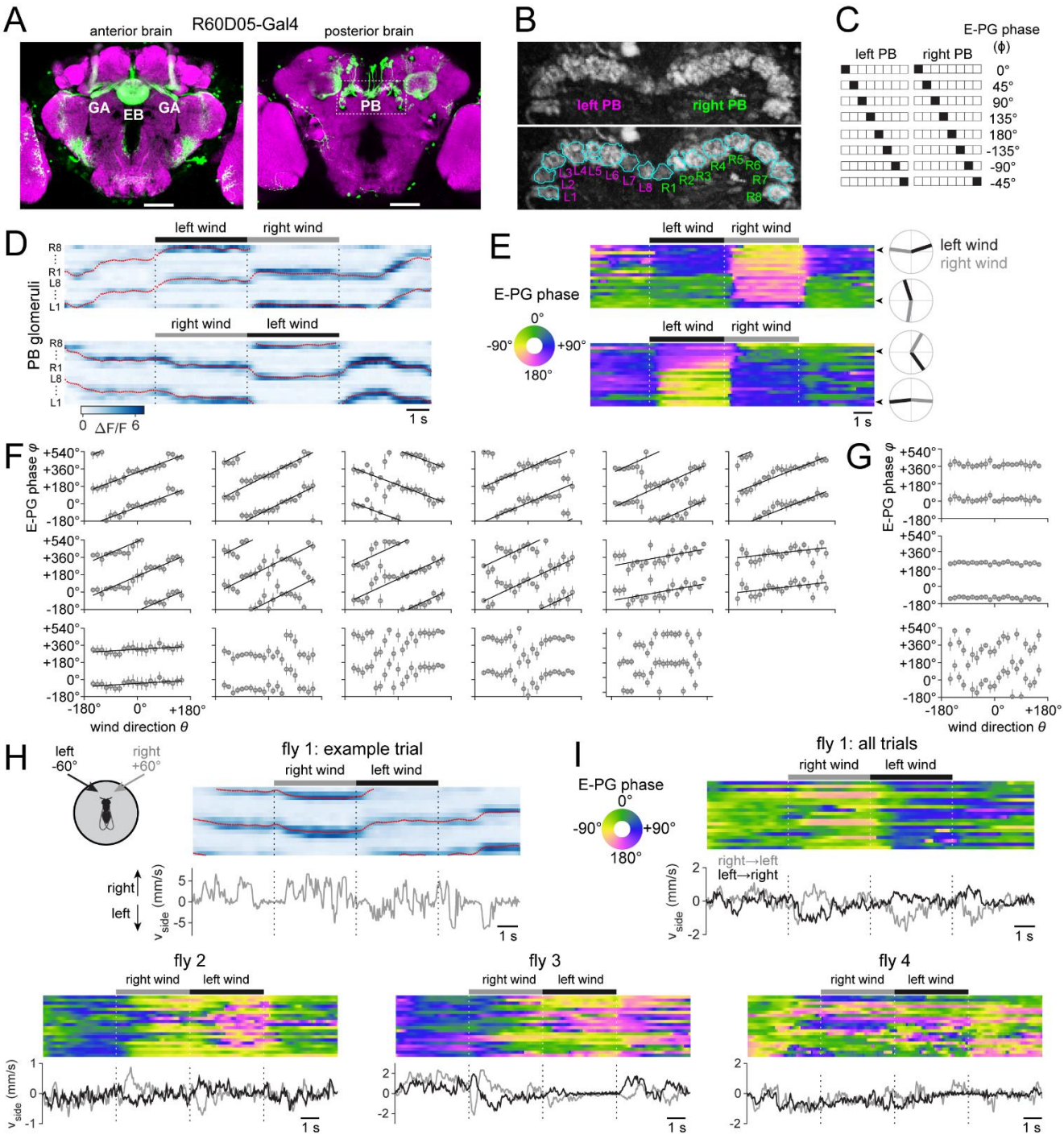

Figure S1. Effects of wind on E-PG neuron ensemble activity. Related to Figure 1

(A) Gal4 line used to drive GCaMP6f in E-PG neurons. EB: ellipsoid body, GA: gall, PB: protocerebral bridge. Box indicates imaging window in (B). Scale bar: 50 µm. Image from FlyLight (Jenett et al., 2012; http://flweb.janelia.org/cgi-bin/flew.cgi).

(B) E-PG neuron axon terminals in the PB, viewed from the posterior side. ROIs show the 16 PB glomeruli (Wolff et al., 2015).

(C) Schematic of E-PG phases in the PB, viewed from the posterior side. Black indicates the center of the bump.

(D) Two example trials from the same fly showing bump phase (red) overlaid with GCaMP6f ΔF/F (colormap). E-PG phase is double-plotted for illustrative purposes, here and in Figures S1H and S2H-I.

(E) Two examples of a spontaneous change in the offset between E-PG phase and wind direction. We also observed one case where the bump/wind relationship changed spontaneously for only one of the two wind directions (data not shown).

(F) Mean E-PG phase versus wind direction for all flies. Error bars are angular deviation. Flies are sorted based on goodness-of-fit (GOF; see Methods). In all the flies where GOF was significant (see Methods), we show fits to $\varphi = [a \cdot \theta + \varphi_0] \pmod{360^\circ}$.

(G) Three control flies where the wind tube rotated but no air was flowing. GOF was not significantly different from shuffled data.

(H-I) We delivered wind from ±60° in open-loop as a fly walked on a spherical treadmill.

(H) Top: E-PG phase (red) overlaid with ΔF/F. Bottom: fly's sideways velocity.

(I) For each fly, top panel shows E-PG phase for all (right wind →left wind) trials. Bottom panel shows mean sideways velocity over all the trials (right →left, left →right). Flies 1 and 2 turn upwind at wind onset, while fly 3 turns downwind at wind onset.

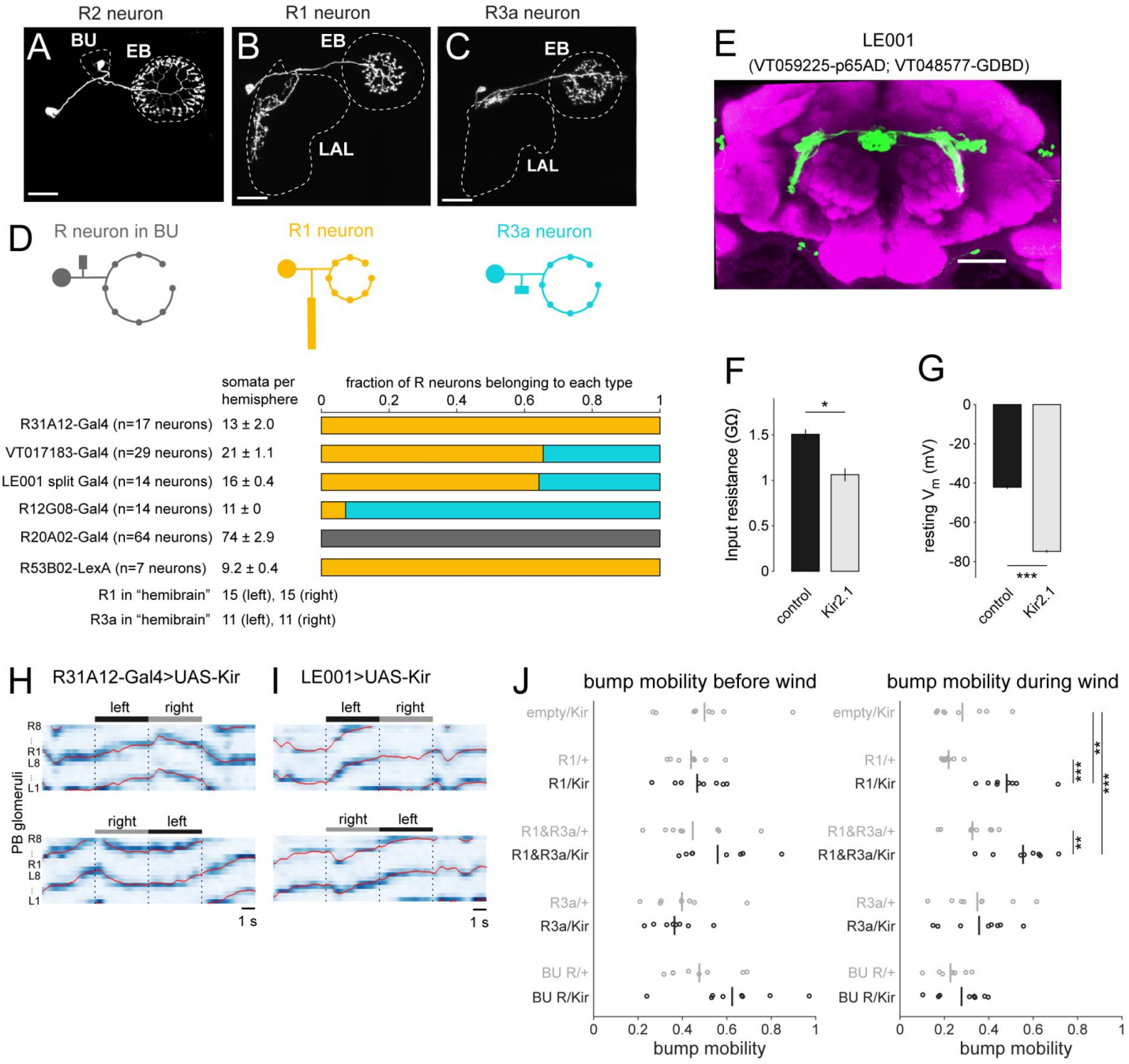

Figure S2: R neuron Gal4 lines and effects of Kir silencing. Related to Figure 2

(A) MCFO labeling of a single R2 neuron with dendrites in the bulb (BU). Reproduced from Fisher et al. (2019). Scale bar: 20 µm.

(B-C) MCFO labeling of a single R1 neuron and R3a neuron, similar to Figure 2A,B. Scale bar: 20 µm.

(D) Representation of different R neuron types in each driver line, based on counting single-cell MCFO clones (n=number of clones examined) or single-cell biocytin fills (n=number of cells filled, for R53B02-LexA only). Data for R20A02-Gal4 are described in Fisher et al. (2019). Somata per hemisphere (mean ± s.e.m.) is indicated at left. Soma counts for R31A12-Gal4 and R12G08-Gal4 are from Omoto et al. (2018); counts for R1/R3a are from the 'hemibrain' dataset of Xu et al. (2020).

(E) Expression pattern of the split-Gal4 line LE001 that was used to target both R1 and R3a neurons. Image is a max *z*-projection of a confocal stack, with GFP immunostaining in green, neuropil counterstain (nc82) in magenta. Scale bar: 50 µm.

(F-G) R1 neuron input resistance and resting potential (n=9 control neurons, n=4 Kir2.1-expressing neurons, mean ± SEM), *p =0.045, Wilcoxon rank-sum test; ***p =4×10^{-6}, two-sample *t*-test. Kir2.1 should not be treated as completely "silencing" a neuron, because a large excitatory current can always – in principle – overcome hyperpolarization and decreased input resistance.

(H) Two trials from a fly where R1 neurons expressed Kir2.1. Note that wind has little or no effect on the bump phase (red).

(I) Two trials from a fly where R1 and R3a neurons expressed Kir2.1. Again, wind has little or no effect. Compare with Figure S1D.

(J) Same as Figure 2G but with a separate datapoint for each fly. Significance testing as in Figure 2G.

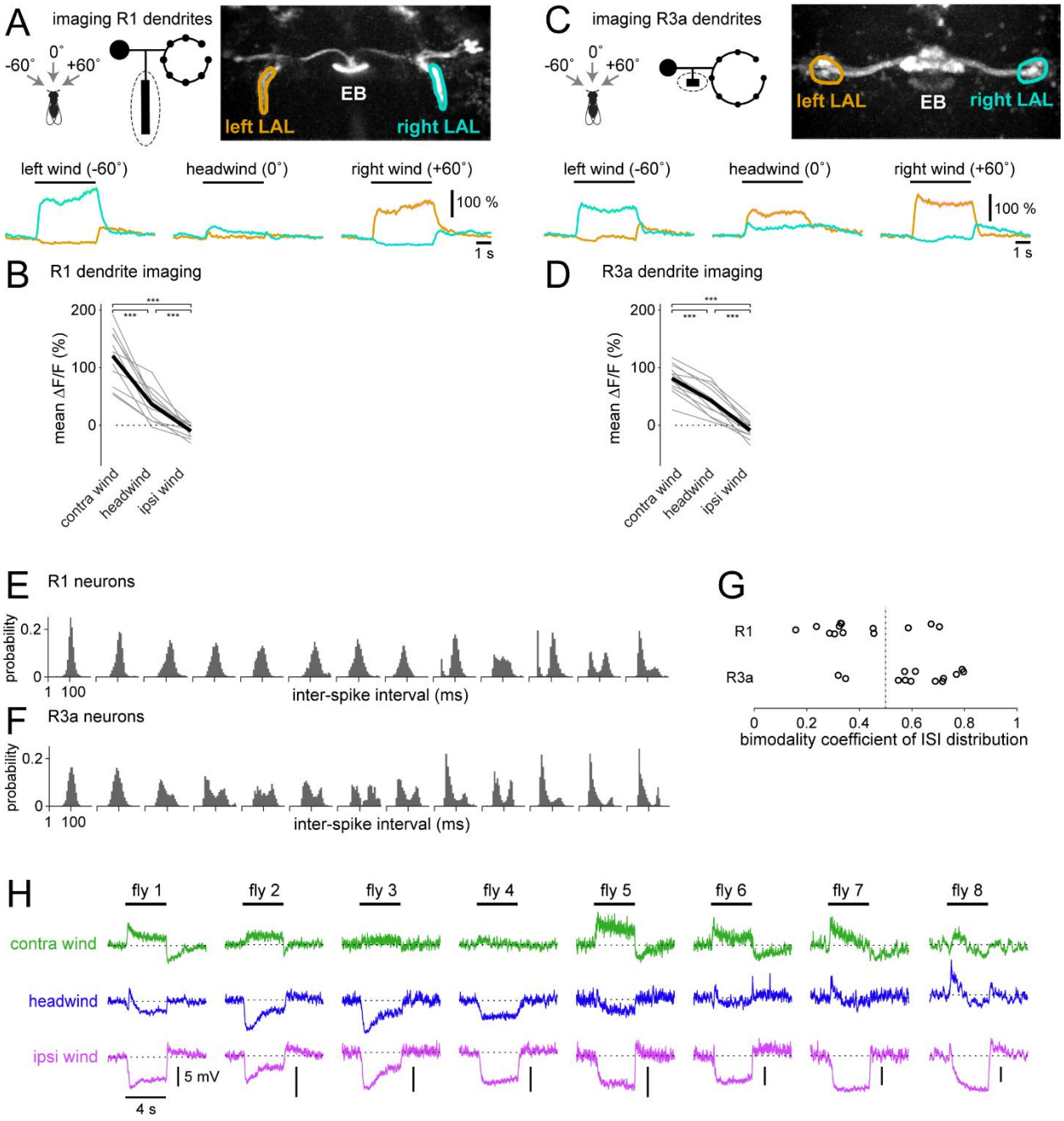

Figure S3: Dendritic calcium responses and spike burstiness of R1/R3a neurons. Related to Figure 3

(A) R1 neuron dendrites in the LAL were imaged while wind was delivered from three directions. Image at right shows GCaMP6f fluorescence in an example brain, with left and right ROIs circled. Traces below show mean changes in fluorescence for each wind direction for these two ROIs, mean ± SEM across trials (n=20 trials).

(B) Population summary of R1 wind response across all the flies ($p=3.5\times10^{-10}$, one-way repeated measures ANOVA followed by paired *t*-test with Bonferroni correction; n = 12 ROIs in 6 flies).

(C-D) Same but for R3a neurons ($p=1.3\times10^{-12}$, one-way repeated measures ANOVA followed by paired *t*-test with Bonferroni correction; n = 12 ROIs in 6 flies).

(E) Inter-spike interval (ISI) distributions for R1 neurons. Note the log scale of the *x*-axis. Each plot represents a different neuron, sorted in increasing order of bimodality coefficients.

(F) Same but for R3a neurons.

(G) Bimodality coefficients of all R1 (n=13 neurons) and R3a (n=13 neurons) where dye-fills were available (**p=0.004, Wilcoxon rank-sum test). Dashed line represents our empirical threshold for classifying a neuron as R1 or R3a when no fill was available. This type of classification pertains only to the cells indicated with asterisks in Figure S4.

(H) R1 neuron membrane potential responses to three wind directions (-60°, 0°, +60°). Each trace is a median-filtered membrane potential (50 ms window) averaged over multiple trials. Dotted line indicates the mean membrane potential before wind onset. Note that at wind offset, there is often a response which is opposite to the response at wind onset. All R1 neurons from Figure 3 are shown here, except for one that did not show significant wind responses.

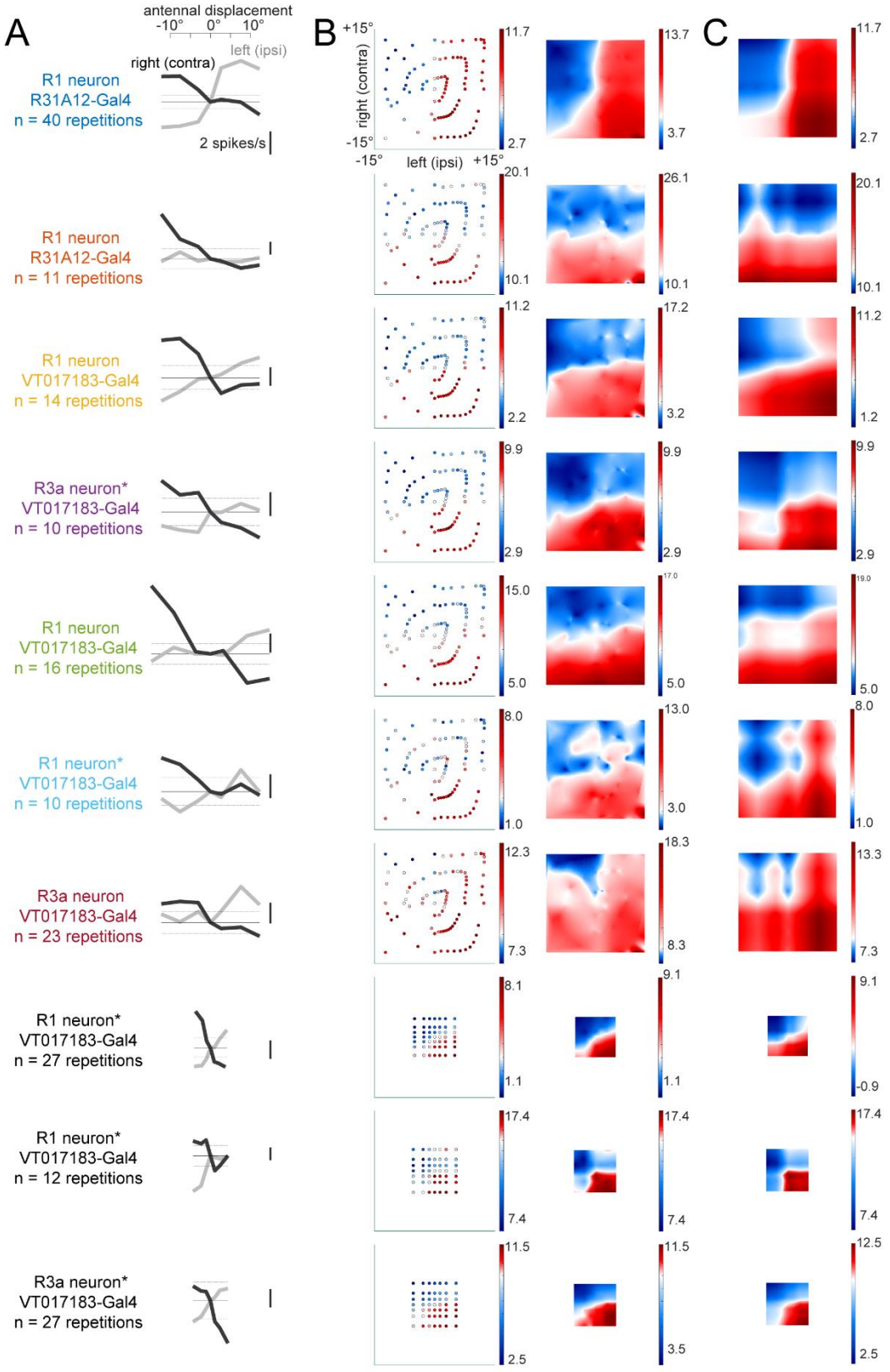

Figure S4: R neuron responses to independent displacements of the two antennae. Related to Figure 5
(A) Responses of all recorded R1/R3a neurons to unilateral displacements of the left antenna (gray) or the right antenna (black). The horizontal line is each cell's mean firing rate when both antennae are at rest (±95% confidence interval). All the neurons were recorded from the left hemisphere. Vertical scale bars denote 2 spikes/s. The first 7 cells appear in Figure 5, and the label colors match the corresponding traces in Figure 5F, G. The last 3 cells do not appear in Figure 5 because we used a smaller stimulus set for these cells. The Gal4 line used to target each cell is indicated, along with the number of repetitions per stimulus condition.
(B) Left: scatterplots show responses of each neuron for all tested combinations of left and right displacements. Right: continuous maps obtained by 2D-interpolation of these scatterplots. Color keys indicate firing rate ranges (in spikes/s).
(C) Predicted bilateral responses, obtained by linearly combining each cell's responses to unilateral stimuli alone, then interpolating.

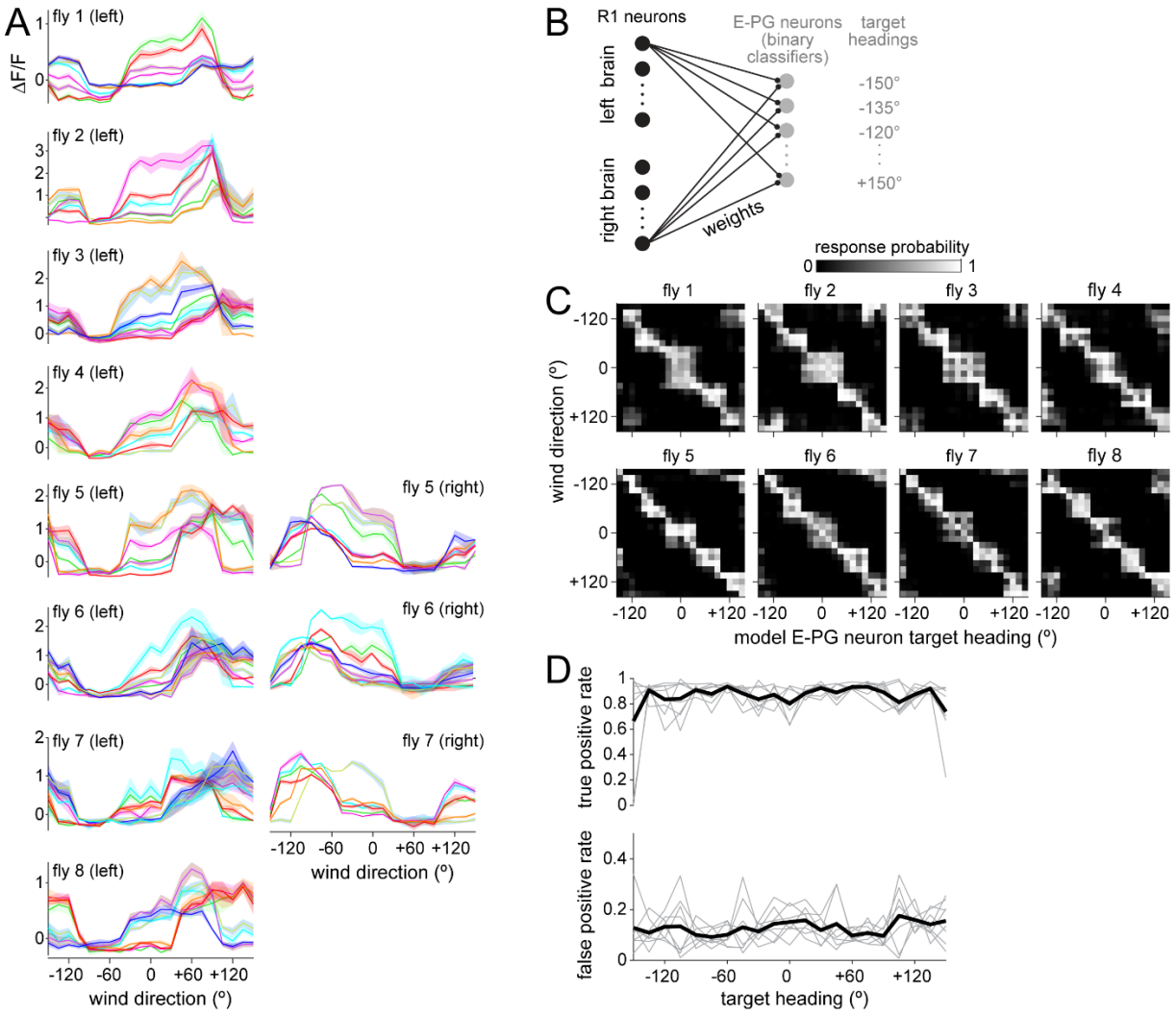

Figure S5: Population imaging of R1 neuron somata. Related to Figure 6

(A) Peak ΔF/F versus wind direction for all the flies. Flies 5-7 were imaged in both the left and right hemisphere; the other flies were imaged in the left hemisphere only.

(B) Schematic of the model network. We created 21 binary classifiers (model E-PG neurons), one for each wind direction in our data set. Every left and right R1 neuron is connected to each model E-PG neuron (not all connections are drawn in the schematic). Connection weights are adjusted so that each model E-PG neuron responds as accurately as possible to one heading (its "target heading"), and no other headings, with different classifiers assigned to different headings. We assume that headings map linearly onto wind directions.

(C) Response probability of each model E-PG neuron (each column) in response to wind from different directions (each row) for all flies. For flies where only left hemisphere R1 data was available, we mirrored the left-side R1 data to simulate R1 neurons on the right side. Response probabilities are shown in grayscale.

(D) True positive rate (top) and false positive rate (bottom) for each model E-PG neuron. Gray lines indicate individual flies (n=8) and the black line indicates the mean across flies.

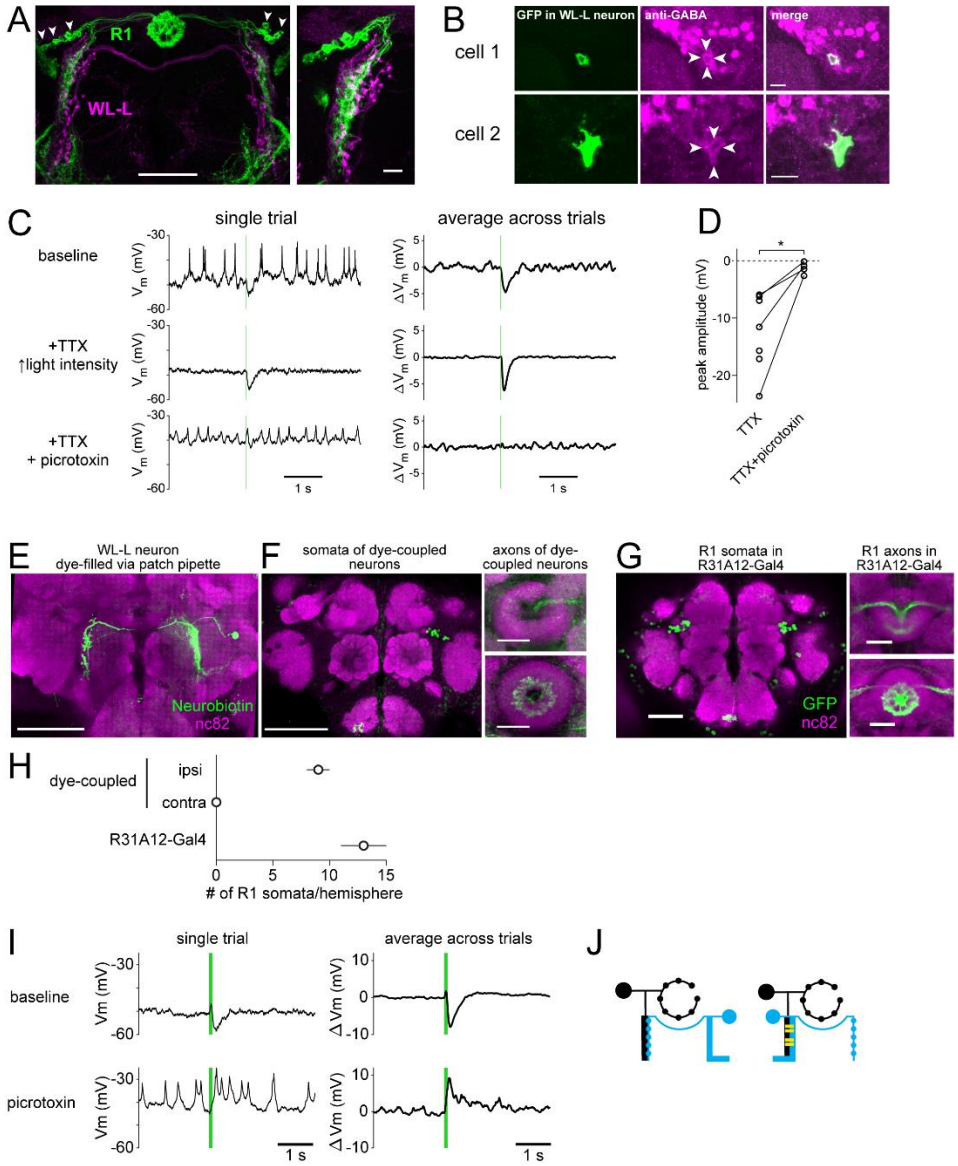

Figure S6: Functional connectivity between WL-L and R1 neurons. Related to Figure 7

(A) Max *z*-projection of a confocal stack of a brain where R1 neurons express GFP and WL-L neurons express CsChrimson::mCherry. Arrowheads indicate R1 somata. Scale bar: 50 µm. Right: enlarged portion of the left LAL. Scale bar: 10 µm.

(B) GABA immunostaining in WL-L neuron somata. GABA immunostaining is weak but above background. It seems likely that WL-L neurons are GABAergic, but cytoplasmic GABA concentrations are relatively low in these cells.

(C) Additional example R1 neuron responses to WL-L photostimulation. The green bar indicates the light pulse (10 ms).

(D) Peak inhibitory postsynaptic potential amplitude in R1 neurons during WL-L photostimulation, in either TTX alone or else TTX+picrotoxin (*p=0.01, two-sample *t*-test; n = 7 recordings in TTX, of which 4 were held long enough to test picrotoxin).

(E) Neurobiotin fill of a WL-L neuron (max z-projection of a confocal stack). Scale bar: 50 µm.

(F) Left: Another confocal section of the same brain as in (E), showing dye-coupled somata of putative R1 neurons in the same brain hemisphere as the filled WL-L neuron. Scale bar: 50 µm. Right: Axons in the inner posterior domain of the EB (top: anterior EB, bottom: posterior EB). Scale bars: 20 µm. Axons in the EB were observed in 8 of 8 flies with WL-L recordings > 10 min. Of these 8, 5 had high enough signal-to-noise ratio to determine that the axons entered the central canal of the EB on the ipsilateral side.

(G) R1 neurons expressing GFP under the control of R31A12-Gal4. The similarity to (F) supports the conclusion that the dye-coupled neurons in (F) are R1 neurons. Image from FlyLight (Jenett et al., 2012; http://flweb.janelia.org/cgi-bin/flew.cgi).

(H) Number of dye-coupled somata dorsolateral to the antennal lobe (ipsi- or contralateral to the recorded WL-L soma, mean ± SEM per hemisphere, n=8 flies with recording >10 min). Soma count from R31A12-Gal4 shown for comparison (from Omoto et al., 2018).

(I) Example R1 neuron response to WL-L photostimulation showing depolarization followed by hyperpolarization (green bar shows 100 ms light pulse). Note that we used a stronger light (250 µW/mm^2) and a longer light pulse for this experiment compared to the experiments in Figure 7. Left: single trial examples of baseline and after 5 µM picrotoxin. Right: Average across trials (n=20) for this neuron. Depolarization persists in picrotoxin, implying that the excitatory response is not due to disinhibition.

(J) Summary schematic. Left: a WL-L neuron forms GABAergic axon-dendritic synapses with R1 neurons in the opposite hemisphere. Right: a WL-L neuron forms dendrodendritic electrical synapses with R1 neurons in the same hemisphere.

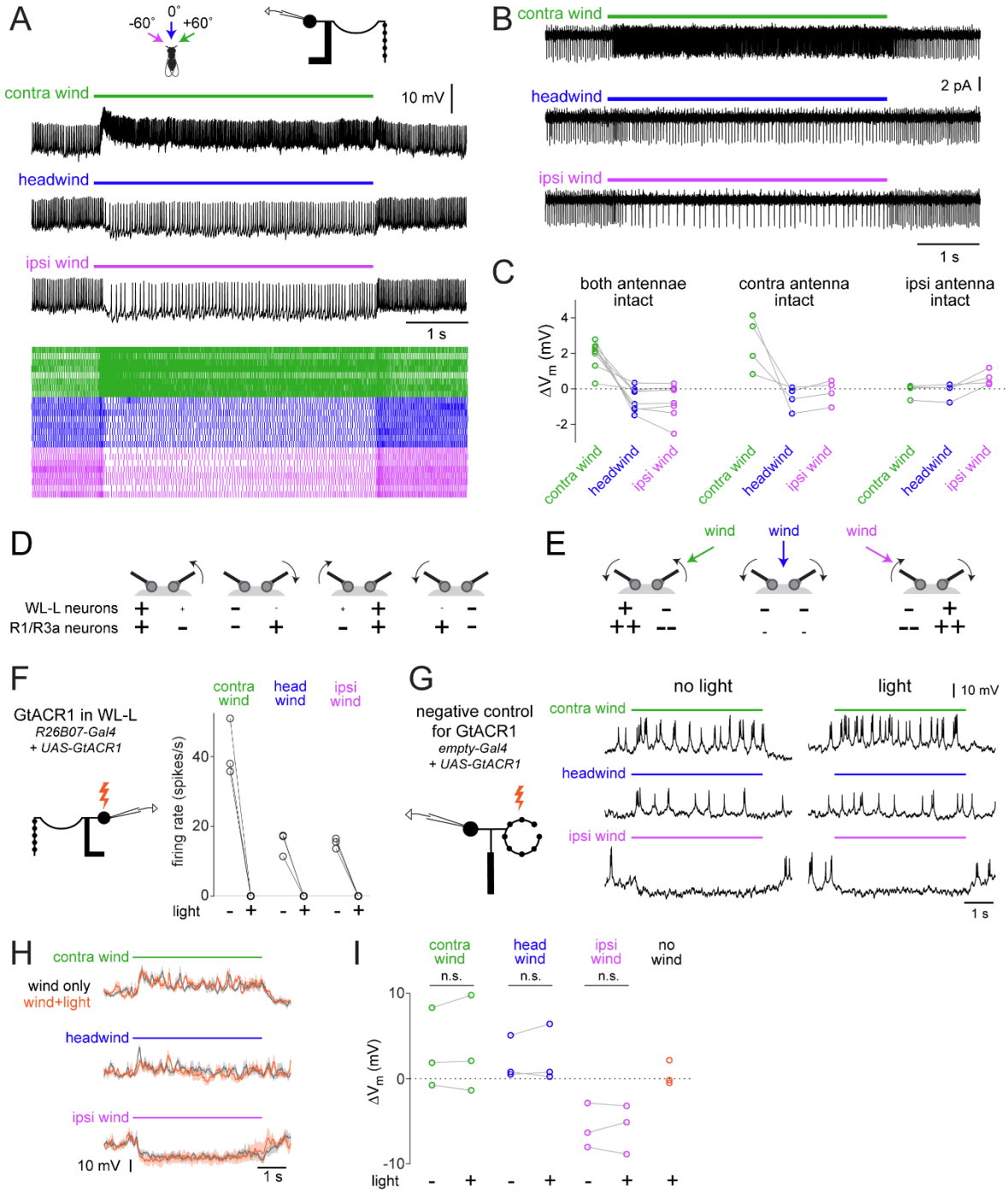

Figure S7: Wind responses in WL-L neurons. Related to Figure 8

(A) Additional example whole-cell recording from an WL-L neuron.

(B) Example of cell-attached recording from an WL-L neuron. Note the high baseline firing rate in this cell type even in cell-attached mode; this demonstrates that the high baseline firing rate in these cells is not an artifact of the whole-cell recording configuration.

(C) Effect of antennal manipulation on WL-L wind responses, here showing voltage (rather than spiking, as in Figure 8D). The interaction between antennal condition (both intact/contra intact/ipsi intact) and wind direction (contra/head/ipsi, within-subject factor) was significant ($p=0.006$; two-way repeated measures ANOVA). The interaction term was not significant for both antennae intact vs. contra intact ($p=0.76$), but was significant for both antennae intact vs. ipsi intact ($p = 0.0001$; two-way repeated measures ANOVA).

(D) Schematic WL-L and R1/R3a responses to unilateral antennal displacements.

(E) Schematic of WL-L and R1/R3a responses to wind-evoked bilateral antennal displacements.

(F) Wind responses of GtACR1+ WL-L neurons with and without light (n=3 flies; 0.04 - 5 $\mu W/mm^2$, light intensity was different for different WL-L recordings but spiking was completely suppressed in all cases; see Methods).

(G) Example R1 neuron recording in the control genotype (where GtACR1 is not expressed in WL-L neurons).

(H) Mean membrane potential of the R1 neuron shown in (G) with and without light (gray; mean ± SEM; 8 trials each condition).

(I) R1 wind responses with and without light in the control genotype. Responses are averaged over the stimulus period and expressed as changes from baseline (n = 3 neurons). Light had no significant effects (paired *t*-tests).

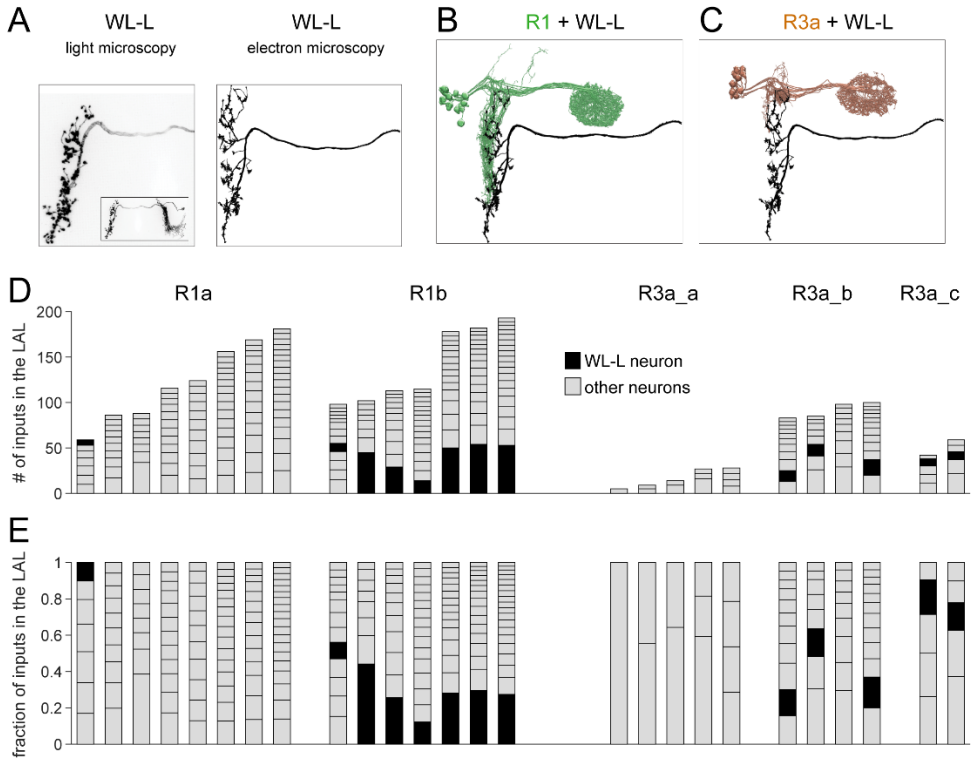

Figure S8: Synaptic connectivity between WL-L neuron and R1/R3a neurons at the EM level. Related to Figure 8
(A) Left: light microscopy (LM) image is a single-cell MCFO labeling of a WL-L neuron axon (max z-projection of a confocal stack). Inset shows the entire neuron. Right: electron microscopy (EM) image shows the axon of a neuron in the right hemisphere of the FlyEM neuPrint 'hemibrain' v1.0.1 skeleton viewer (body ID: 1386849677; Xu et al., 2020). Based on LM/EM correspondence, we identify this neuron in the EM dataset as WL-L. The left hemisphere is not included in the EM volume, and so the soma and dendrite cannot be recovered.
(B) All the R1 neurons that innervate the right LAL in the FlyEM dataset (n = 15 neurons) overlaid with the WL-L axon.
(C) All the R3a neurons that innervate the right LAL in the FlyEM dataset (n = 11 neurons) overlaid with the WL-L axon.
(D) Number of synaptic inputs that individual R1 neurons and R3a neurons receive in the right LAL. Black: WL-L neuron; gray: all the other neurons. Each stacked bar represents a different R neuron. The FlyEM Project has subdivided R1 neurons into R1a and R1b, and R3a neurons into R3a_a, R3a_b, and R3a_c. Note that WL-L is the largest input to most R1b neurons, but it does not provide input to most R1a neurons. WL-L also provides input to several R3a neurons.
(E) Same as in (D) but with each bar normalized by the total number of inputs in the LAL.
For (D) and (E), presynaptic neurons that make 3 synapses or fewer have been omitted, based on the recommendation of Xu et al. (2020).

Table S1: Previous studies using the term 'R1 neurons', organized by the Gal4 line used. Related to Figure 2

The term 'R1 neurons' has been used to refer to various R neuron types. In the current study, we use the terminology of Omoto et al. (2018). Full citations appear in the References.

Gal4 line used to target R neurons	**R neuron dendrites in BU and/or LAL**	**R neuron type according to Omoto et al. (2018)**	**Previous studies using this Gal4 line**
c105	LAL	R1	Renn…Taghert (J. Neurobiol., 1999) Baker…Armstrong (J. Comp. Neurol., 2007) Neuser…Strauss (Nature, 2008) Chen … Chien (Dev. Neurobiol., 2011) Kuntz…Strauss (Learn. Memory, 2012) Lin…Chiang (Cell Rep., 2013) Martin-Pena…Ferrus (Eur. J. Neurosci., 2014) Kuntz…Strauss (Curr. Biol., 2017) Kottler … Hirth (Curr. Biol., 2019)
c561	LAL	R1	Renn…Taghert (J. Neurobiol., 1999)
198Y	?	?	Renn…Taghert (J. Neurobiol., 1999)
52y	BU	R5	Young…Armstrong (J. Comp. Neurol., 2010)
796	BU	many types	Martin-Pena…Ferrus (Eur. J. Neurosci., 2014)
R15B07	BU	R3d/R3p/R4d	Ofstad…Reiser (Nature, 2011) Dus…Suh (Nat. Neurosci., 2013) Shiozaki…Kazama (Nat. Neurosci., 2017) Xie…Kolodkin (eLife, 2017)
R28D01	BU	R3m	Ofstad…Reiser (Nature, 2011) Dus…Suh (Nat. Neurosci., 2013)
R31A12	LAL	R1	Omoto…Hartenstein (Front. Neural Circuit, 2018) current study
R32A11	LAL	?	Franconville…Jayaraman (eLife, 2017)[1]
R75H04	BU/LAL	many types	Franconville…Jayaraman (eLife, 2017)[2]
VT39763	BU	R3?	Lin…Chiang (Cell Rep., 2013)
tim(UAS)-Gal4	?	?	Liang…Taghert (Neuron, 2019)
VT059225-AD, VT048577-DBD	LAL	R1/R3a	current study

[1] The authors used the term 'L-Em' to refer to neurons labeled in *R32A11-Gal4* line.
[2] The authors used the term 'L-Ei' to refer to neurons labeled in *R75H04-Gal4* line.